Contribution from the Department of Chemistry,
Faculty of Science, Tohoku University, Aoba, Aramaki, Sendai 980, Japan

Asymmetric Distortion of Bis(μ-oxo)bis(oxotungstate(V)) Complexes. Crystal Structure of Bis(μ-oxo)(μ-*N*,*N*′-(*R*)-propylenediaminetetraacetato)bis(oxotungstate(V))

Shinji Ikari, Yoichi Sasaki,* and Tasuku Ito*

Received May 12, 1989

$Mo^{V}_2(O)_2(\mu\text{-}O)_2$ complexes are known to be distorted asymmetrically when optically active ligands are coordinated. The distortion of the $W^{V}_2(O)_2(\mu\text{-}O)_2$ complexes has been compared with that of the Mo^{V} dimers. Extent of the asymmetric distorsion is found to be smaller for the W^{V}_2 complexes than for the Mo^{V}_2 ones, as evidenced by the following three facts. (i) The various torsion angles of the new complex $[W_2(O)_2(\mu\text{-}O)_2(\mu\text{-}R\text{-pdta})]^{2-}$ (*R*-pdta = (*R*)-propylenediamine-*N*,*N*,*N*′,*N*′-tetraacetate(4-)) as determined by the X-ray crystal structural analysis are smaller than the corresponding angles of the Mo_2 complex. Crystals of $Ba[W_2(O)_2(\mu\text{-}O)_2(\mu\text{-}R\text{-pdta})]\cdot 6H_2O$ ($C_{11}H_{26}N_2O_{18}BaW_2$) are triclinic, space group *P*1, with $a = 7.625$ (1) Å, $b = 11.882$ (2) Å, $c = 7.133$ (1) Å, $\alpha = 98.623$ (9)°, $\beta = 94.288$ (9)°, $\gamma = 116.922$ (8)°, $V = 562.2$ (1) Å^3, and $Z = 1$. The structure was solved by use of 4895 unique reflections with $|F_o| > 3\sigma(F_o)$ to give $R = 0.036$. (ii) Circular dichroism spectra of the W_2–*R*-pdta complex show peaks with magnitudes smaller than those of the corresponding peaks of the Mo_2–*R*-pdta complex. (iii) Dynamic ^{13}C NMR analysis of the asymmetric inversion ($\Delta \rightleftarrows \Lambda$) of the W_2–edta (edta = ethylenediaminetetraacetate(4-)) gives $k = (2.87 \pm 0.06) \times 10^2$ s^{-1} (25 °C), $\Delta H^{\ddagger} = 36 \pm 2$ kJ mol^{-1}, and $\Delta S^{\ddagger} = -53 \pm 5$ J K^{-1} mol^{-1}. The $\Delta H^{\ddagger}$ is smaller than the one for the inversion of the Mo_2–edta complex, suggesting smaller amplitude of the inversion. The higher extent of the covalent character of the W^{V}_2 complexes may account for the observations.

Introduction

Both molybdenum(V) and tungsten(V) give dimeric complexes with the core $M_2(O)_2(\mu\text{-}O)_2$ in aqueous media.[1-4] Complexes with this core have a heavily distorted octahedral environment around each metal ion. We have previously shown that two distorted octahedra of the $Mo_2O_4^{2+}$ complexes are twisted with respect to each other around the metal–metal axis to give asymmetric arrangement when optically active ligands such as (*R*)-propylenediamine-*N*,*N*,*N*′,*N*′-tetraacetate(4-) (*R*-pdta) and various amino carboxylate ions are coordinated.[5,6] The optically active distortion is also expressed by the torsion of two basal edges (see Figure 1).

It is suggested that in the case of the pdta complex asymmetric distortion is induced by the fixed pseudo-gauche conformation of the N–C–C(CH_3)–N bridge (methyl group takes equatorial orientation). The conformational inversion is not possible due to steric hindrance of the methyl group. On the other hand,the pseudo-gauche conformation is rapidly inverted in aquous solution in the case of the corresponding edta (ethylenediaminetetraacetate(4-)) complex. This is regarded as asymmetric inversion ($\Delta \rightleftarrows \Lambda$) (Figure 1). The kinetic parameters of the inversion of $[Mo_2(O)_2(\mu\text{-}O)_2(\mu\text{-edta})]^{2-}$ have been obtained by Blackmer and co-workers, by the use of variable-temperature ^{13}C NMR spectroscopy.[7]

It is interesting to know how the asymmetric distortion is affected on going from molybdenum(V) to tungsten(V). We report here the first optically active complex of $W_2O_4^{2+}$, $[W_2(O)_2(\mu\text{-}O)_2(\mu\text{-}R\text{-pdta})]^{2-}$, and compare the extent of optically active distortion with that of the $Mo_2O_4^{2+}$ complex by the use of an X-ray structural analysis and circular dichroism spectrum. Inversion of the N–C–C–N bridge in $[W_2(O)_2(\mu\text{-}O)_2(\mu\text{-edta})]^{2-}$ has also been investigated in order to compare a dynamic aspect of the asymmetric distortion with that of the corresponding Mo^{V}_2 complex.

Experimental Section

1. Preparation of the Complexes. (1) Sodium Salt of (μ-(*R*)-Propylenediamine-*N*,*N*,*N*′,*N*′-tetraacetato)bis(μ-oxo)bis(oxotungstate(V)), $Na_2[W_2(O)_2(\mu\text{-}O)_2(\mu\text{-}R\text{-pdta})]\cdot NaClO_4\cdot 3H_2O$. The ammonium salt of the oxalato complex of tungsten(V)[8] (1.4 g) was added to an aqueous solution (35 mL) of (*R*)-propylenediaminetetraacetic acid (H_4(*R*-pdta)) (1.3 g) and sodium acetate (1.3 g). The solution was kept at 80 °C for ca. 10 min with stirring and mixed with an aqueous solution (10 mL) of $CaCl_2\cdot 2H_2O$ (2.4 g). The precipitate (CaC_2O_4) was filtered off. The red filtrate was diluted after 1 day with a large amount of water and was adsorbed on a column of QAE-Sephadex A-25 resin in the Cl^- form. The column was washed with water. The brown band was then eluted with 0.15 M $NaClO_4$. The eluate was concentrated, and $NaClO_4$ was removed. On addition of ethanol to the concentrate, orange air-stable crystals of $Na_2[W_2(O)_2(\mu\text{-}O)_2(\mu\text{-}R\text{-pdta})]\cdot NaClO_4\cdot 3H_2O$ were obtained; yield 0.73 g (42%). Anal. Calcd for $C_{11}H_{20}N_2O_{19}ClNaW_2$: C, 13.81; H, 2.11; N, 2.93. Found: C, 13.30; H, 2.77; N, 3.12. IR (cm^{-1}): 3420 br, 2980 w, 1655 s, 1445 w, 1383 s, 1245 w, 1121 m, 1088 m, 950 s, 909 m, 879 w, 845 w, 755 m, 625 m, 515 m, 456 m, 405 m.

(2) Other Materials. A racemic mixture of the pdta complex, $Na_2[W_2(O)_2(\mu\text{-}O)_2(\mu\text{-}rac\text{-pdta})]$, was prepared by the use of racemic H_4pdta instead of H_4(*R*-pdta). The edta complex, $Na_2[W_2(O)_2(\mu\text{-}O)_2(\mu\text{-edta})]$,[9] was prepared as previously described.[10] *rac*- and (*R*)-propylenediaminetetraacetic acids (H_4pdta) were prepared according to the reported method.[11]

2. Measurements. Ultraviolet and visible absorption spectra were measured with Hitachi 330 and Hitachi 340 spectrophotometers. CD spectra were recorded on a JASCO J-40 automatic recording spectropolarimeter. Infrared absorption spectra were measured by a JASCO IR-810 spectrophotometer in KBr pellets at room temperature. ^1H and ^{13}C NMR spectra were measured on a JEOL GSX-270 FT-NMR spectrometer at 270 and 67.9 MHz in D_2O, respectively, at 25 °C. The variable-temperature ^{13}C NMR spectra were measured at 22.5 MHz in D_2O by a JEOL FX-90Q spectrometer with a random-noise ^1H decoupler and a variable-temperature controller. Chemical shifts in the ^1H and ^{13}C

Table I. Crystallographic Data for $Ba[W_2(O)_2(\mu\text{-}O)_2(\mu\text{-}R\text{-pdta})]\cdot 6H_2O$

$C_{11}H_{14}N_2O_{12}BaW_2\cdot 6H_2O$	fw = 965.34
$a = 7.625$ (1) Å	space group *P*1 (No. 1)
$b = 11.882$ (2) Å	$T = 13$ °C
$c = 7.133$ (1) Å	$\lambda = 0.71069$ Å
$\alpha = 98.623$ (9)°	$\rho_{obsd} = 2.852$ g cm^{-3} [a]
$\beta = 94.288$ (9)°	$\rho_{calcd} = 2.852$ g cm^{-3}
$\gamma = 116.922$ (8)°	$\mu = 126.9$ cm^{-1}
$V = 562.2$ (1) Å^3	$R(F_o)$ [b] = 0.036
$Z = 1$	$R_w(F_o^2)$ [c] = 0.040

[a] In $Br_2CHCHBr_2$–$CHBr_3$. [b] $R = \sum||F_o| - |F_c||/\sum|F_o|$. [c] $R_w = [\sum w(|F_o| - |F_c|)^2/\sum|F_o|^2]^{1/2}$; $w = 1/\sigma^2(|F_o|)$.

(1) Cotton, F. A.; Wilkinson, G. *Advanced Inorganic Chemistry*, 5th ed.; Wiley: New York, 1988; pp 831.
(2) Greenwood, N. N.; Earnshaw, A. *Chemistry of the Elements*; Pergamon Press: Oxford, England, 1984, pp 1167.
(3) Stiefel, E. I. *Prog. Inorg. Chem.* **1977**, *22*, 1-223.
(4) Dori, Z. *Prog. Inorg. Chem.* **1981**, *28*, 239-307.
(5) Suzuki, K. Z.; Sasaki, Y.; Ooi, S.; Saito, K. *Bull. Chem. Soc. Jpn.* **1980**, *53*, 1288-1298.
(6) Kojima, A.; Ooi, S.; Sasaki, Y.; Suzuki, K. Z.; Saito, K.; Kuroya, H. *Bull. Chem. Soc. Jpn.* **1981**, *54*, 2457-2465.
(7) Blackmer, G. L.; Johnson, K. J.; Roberts, R. L. *Inorg. Chem.* **1976**, *15*, 596-601.
(8) Collenberg, O. *Z. Anorg. Allg. Chem.* **1918**, *102*, 247-276.
(9) Novak, J.; Podlaha, J. *J. Inorg. Nucl. Chem.* **1974**, *36*, 1061-1065.
(10) Ikari, S.; Sasaki, Y.; Nagasawa, A.; Kabuto, C.; Ito, T. *Inorg. Chem.* **1989**, *29*, 1248-1254.
(11) Dwyer, F. P.; Garvan, F. L. *J. Am. Chem. Soc.* **1959**, *81*, 2955-2957.

0020-1669/90/1329-0053$02.50/0

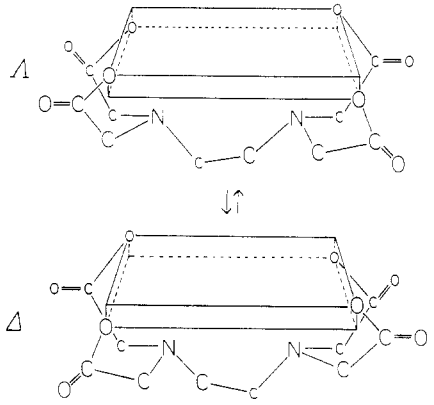

Figure 1. Conformational inversion of $[M_2(O)_2(\mu\text{-}O)_2(\mu\text{-edta})]^{2-}$(M = Mo, W) (core structure, $M_2(O)_2(\mu\text{-}O)_2$, omitted for clarity).

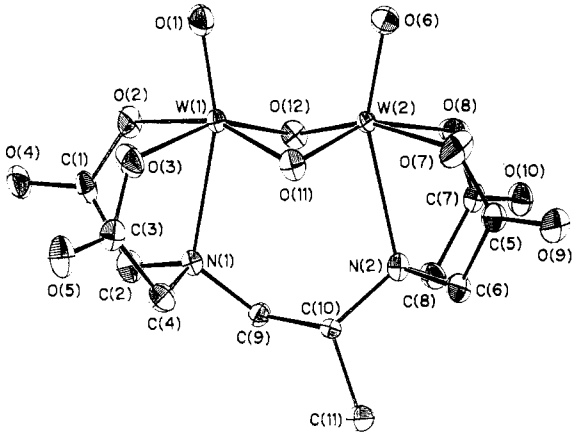

Figure 2. Structure of $[W_2(O)_2(\mu\text{-}O)_2(\mu\text{-}R\text{-pdta})]^{2-}$ ion and its atomic numbering scheme. The thermal elipsoids are drawn at the 50% probability.

NMR spectra were recorded with sodium 3-(trimethylsilyl)propionate-d_4 (TSP), $(CH_3)_3Si(CD_2)_2CO_2^-Na^+$, and sodium 3-(trimethylsilyl)-1-propanesulfonate (DSS), $(CH_3)_3Si(CH_2)_3SO_3^-Na^+$, respectively, as internal references.

3. Crystal Structure Determination. Crystals of the barium salt, $Ba[W_2(O)_2(\mu\text{-}O)_2(\mu\text{-}R\text{-pdta})]\cdot 6H_2O$ for the X-ray structural determination were obtained by slow crystallization from the aqueous solution of the sodium salt containing $BaCl_2$ by adding ethanol. An air-sensitive orange crystal (0.35 × 0.25 × 0.20 mm) of the barium salt was glued with epoxy to the inside of a thin-walled Lindemann glass capillary and mounted on a RIGAKU AFC-5R four-circle diffractometer equipped with a rotating anode (40 kV, 200 mV) using graphite-monochromated Mo Kα radiation (0.71069 Å). Observed intensities were corrected for Lorentz and polarization factors. The unit cell parameters were obtained by a least-squares refinement of the angular settings of 25 high-angle ($2\theta \sim 30°$) reflections. Crystallographic data are listed in Table I. Intensity data ($\pm h,\pm k,+l$) were obtained by using a 2θ–ω scan. A total of 5650 independent reflections in the range $3 < 2\theta < 70°$ were measured at a scanning rate of 4.0° min^{-1} and with scanning range of (1.3 + 0.15 tan θ)°. The intensities of three standard reflections did not vary significantly throughout the data collection. Atomic scattering factors, f, $\Delta f'$, and $\Delta f''$, were taken from ref 12.

The structure was solved by the heavy-atom method and refined by the block-diagonal least-squares method. The function used in the least-squares minimization was $\sum w\{|F_o| - |F_c|\}^2$, where $w = 1/\omega^2(|F_o|)$. Anisotropic temperature factors were applied to all non-hydrogen atoms. Hydrogen atoms were located at the calculated positions. The final refinement gave $R = 0.036$ for 4895 independent reflections having $|F_o| > 3\sigma(F_o)$ and 308 independent parameters. A final difference Fourier synthesis indicated no significant peaks larger than 1.0 e Å^{-3}.

All calculations were performed with the Universal Crystallographic Computer Program System UNICS III[13] on a ACOS-2000 computer at the Computer Center of Tohoku University. Atomic positional parameters are given in Table II. Tables of the hydrogen atomic coordinates

(12) *International Tables for X-Ray Crystallography*; Kynoch: Birmingham, England, 1974; Vol. IV.
(13) Sakurai, T.; Kobayashi, K. *Rigaku Kenkyusho Hokoku* **1979**, *55*, 69–77.

Table II. Positional and Equivalent Isotropic Thermal Parameters for $Ba[W_2(O)_2(\mu\text{-}O)_2(\mu\text{-}R\text{-pdta})]\cdot 6H_2O$[a,b]

atom	x	y	z	B_{eq}, Å^2
W(1)	−32211 (7)	−21050 (4)	−3997 (7)	1.2
W(2)	0	0	0	1.1
Ba	−10650 (9)	27684 (6)	40919 (9)	1.3
O(1)	−4149 (14)	−1735 (9)	1529 (14)	2.1
O(2)	−6041 (12)	−2922 (9)	−2131 (15)	2.2
O(3)	−3974 (16)	−3931 (8)	−102 (14)	2.2
O(4)	−8336 (14)	−4706 (9)	−4056 (16)	2.4
O(5)	−4059 (17)	−5823 (10)	−929 (18)	2.9
O(6)	−254 (14)	880 (9)	1968 (12)	1.9
O(7)	3001 (14)	711 (12)	1115 (14)	2.9
O(8)	964 (16)	1601 (9)	−1405 (14)	2.2
O(9)	6127 (13)	1432 (11)	722 (15)	2.7
O(10)	1945 (14)	2522 (8)	−3864 (14)	1.9
O(11)	−456 (12)	−1685 (8)	305 (13)	1.6
O(12)	−2437 (12)	−687 (8)	−1912 (12)	1.5
N(1)	−2992 (13)	−3236 (9)	−3392 (13)	1.4
N(2)	1576 (13)	−422 (9)	−2700 (13)	1.3
C(1)	−6596 (16)	−3901 (10)	−3554 (17)	1.6
C(2)	−4969 (18)	−3854 (14)	−4639 (19)	2.4
C(3)	−3630 (18)	−4738 (12)	−1168 (19)	1.8
C(4)	−2547 (20)	−4251 (11)	−2806 (21)	2.1
C(5)	4350 (16)	795 (12)	83 (17)	1.8
C(6)	3685 (16)	14 (12)	−1886 (18)	1.9
C(7)	1525 (15)	1615 (10)	−3073 (16)	1.4
C(8)	1515 (18)	398 (10)	−4088 (17)	1.7
C(9)	−1521 (15)	−2499 (10)	−4616 (15)	1.4
C(10)	685 (15)	−1831 (9)	−3790 (15)	1.3
C(11)	1828 (20)	−1930 (13)	−5487 (20)	2.1
$O_w(1)$	−1711 (22)	−6947 (13)	−2144 (17)	3.5
$O_w(2)$	−1613 (17)	4675 (11)	2585 (17)	2.8
$O_w(3)$	−3059 (15)	304 (9)	−5117 (14)	2.3
$O_w(4)$	1865 (21)	3763 (11)	−8283 (20)	3.8
$O_w(5)$	−4793 (15)	−7233 (11)	−5721 (18)	3.1
$O_w(6)$	1356 (28)	−4190 (21)	−9554 (26)	3.8

[a] Atomic numbering is shown in Figure 2. Tungsten and barium atom positional parameters have been multiplied by 10^5, and other positional parameters, by 10^4. [b] $B_{eq} = {}^3/_4\sum_i\sum_j\beta_{ij}\mathbf{a}_i\cdot\mathbf{a}_j$.

Table III. Selected Interatomic Distances and Angles for $[W_2(O)_2(\mu\text{-}O)_2(\mu\text{-}R\text{-pdta})]^{2-}$

Bond Distances (Å)			
W(1)–W(2)	2.5472 (6)		
W(1)–O(1)	1.68 (1)	W(2)–O(6)	1.70 (1)
W(1)–O(2)	2.108 (9)	W(2)–O(7)	2.09 (1)
W(1)–O(3)	2.03 (1)	W(2)–O(8)	2.14 (1)
W(1)–O(11)	1.939 (9)	W(2)–O(11)	1.92 (1)
W(1)–O(12)	2.022 (9)	W(2)–O(12)	1.973 (8)
W(1)–N(1)	2.41 (1)	W(2)–N(2)	2.45 (1)
Bond Angles (deg)			
W(2)–W(1)–O(1)	99.5 (3)	W(1)–W(2)–O(6)	100.3 (3)
W(2)–W(1)–O(2)	134.6 (3)	W(1)–W(2)–O(7)	137.2 (4)
W(2)–W(1)–O(3)	136.2 (3)	W(1)–W(2)–O(8)	134.1 (3)
W(2)–W(1)–O(11)	48.4 (3)	W(1)–W(2)–O(11)	49.0 (3)
W(2)–W(1)–O(12)	49.5 (2)	W(1)–W(2)–O(12)	51.3 (3)
W(2)–W(1)–N(1)	99.4 (2)	W(1)–W(2)–N(2)	103.1 (2)
O(1)–W(1)–O(2)	90.8 (4)	O(6)–W(2)–O(7)	89.8 (5)
O(1)–W(1)–O(3)	95.6 (5)	O(6)–W(2)–O(8)	91.2 (5)
O(1)–W(1)–O(11)	111.0 (4)	O(6)–W(2)–O(11)	113.6 (5)
O(1)–W(1)–O(12)	109.6 (5)	O(6)–W(2)–O(12)	108.1 (5)
O(1)–W(1)–N(1)	160.9 (3)	O(6)–W(2)–N(2)	156.6 (3)
O(2)–W(1)–O(3)	85.6 (4)	O(7)–W(2)–O(8)	86.6 (5)
O(2)–W(1)–O(11)	157.8 (4)	O(7)–W(2)–O(11)	88.8 (5)
O(2)–W(1)–O(12)	85.3 (4)	O(7)–W(2)–O(12)	159.4 (4)
O(2)–W(1)–N(1)	73.4 (4)	O(7)–W(2)–N(2)	73.9 (4)
O(3)–W(1)–O(11)	87.8 (4)	O(8)–W(2)–O(11)	154.8 (4)
O(3)–W(1)–O(12)	153.3 (4)	O(8)–W(2)–O(12)	82.9 (4)
O(3)–W(1)–N(1)	72.9 (4)	O(8)–W(2)–N(2)	71.5 (4)
O(11)–W(1)–O(12)	91.2 (4)	O(11)–W(2)–O(12)	93.3 (4)
O(11)–W(1)–N(1)	84.4 (4)	O(11)–W(2)–N(2)	83.3 (4)
O(12)–W(1)–N(1)	80.5 (4)	O(12)–W(2)–N(2)	85.9 (3)
W(1)–O(11)–W(2)	82.6 (4)	W(1)–O(12)–W(2)	79.2 (4)

Table IV. Torsion Angles (deg) θ_1–θ_4 and ξ for $[M_2(O)_2(\mu\text{-}O)_2(\mu\text{-}R\text{-pdta})]^{2-}$ (M = W, Mo[5,6])[a,b]

compd	θ_1	θ_2	θ_3	θ_4	ξ
$Ba[W_2O_4(pdta)]$	2.7 (5)	3.9 (6)	10.3 (7)	4.9 (3)	7.0 (4)
$Na_2[Mo_2O_4(pdta)]$	5.4 (8)	8.6 (10)	6.8 (11)	5.4 (6)	8.6 (7)

[a] For the definitions of θ_1–θ_4 and ξ, see Figure 3. [b] Estimated standard deviations in parentheses.

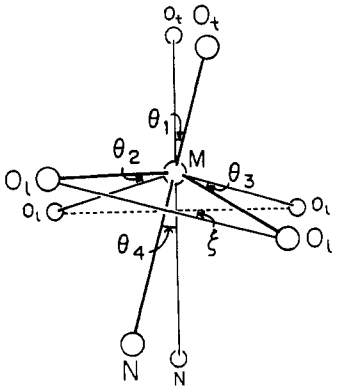

Figure 3. Definition of the torsion angles for $[M_2(O)_2(\mu\text{-}O)_2(\mu\text{-}R\text{-pdta})]^{2-}$ (M = Mo, W). ξ is the torsion angles of the two $O_t \cdots O_t$ axes.

(Table SI), the anisotropic thermal parameters (Table SII), and the structure factors are available as supplementary material.

Results and Discussion

1. Crystal and Molecular Structure of the Complex. Figure 2 shows an ORTEP drawing of the complex anion $[W_2(O)_2(\mu\text{-}O)_2(\mu\text{-}R\text{-pdta})]^{2-}$ together with its atomic numbering scheme. Selected bond distances and angles within the anion are summarized in Table III. The overall structure of the anion is similar to those of the edta complex, $Ba[W_2(O)_2(\mu\text{-}O)_2(\mu\text{-edta})]$,[14] and the *R*-pdta complex of molybdenum(V), $Na_2[Mo_2(O)_2(\mu\text{-}O)_2(\mu\text{-}R\text{-pdta})]$.[6]

The methyl group of $[W_2(O)_2(\mu\text{-}O)_2(\mu\text{-}R\text{-pdta})]^{2-}$ takes equatorial orientation. Therefore, pseudo gauche conformation of the N–C–C(CH_3)–N bridge is fixed and the conformational inversion is not possible due to steric hindrance of the methyl group.

Two distorted octahedra are twisted with respect to each other around the meal–metal axis to give asymmetric arrangement. The direction of the asymmetric distortion is the same as that of $[Mo_2(O)_2(\mu\text{-}O)_2(\mu\text{-}R\text{-pdta})]^{2-}$. The torsion angles around the metal–metal axis in $[W_2(O)_2(\mu\text{-}O)_2(\mu\text{-}R\text{-pdta})]^{2-}$ are compared with those of $[Mo_2(O)_2(\mu\text{-}O)_2(\mu\text{-}R\text{-pdta})]^{2-}$[5,6] in Table IV. The definitions of θ_1, θ_2, θ_3, θ_4, and ξ are given in Figure 3. Except for θ_3 each torsion angle of $[W_2(O)_2(\mu\text{-}O)_2(\mu\text{-}R\text{-pdta})]^{2-}$ is smaller than the corresponding one of $[Mo_2(O)_2(\mu\text{-}O)_2(\mu\text{-}R\text{-pdta})]^{2-}$. It is concluded that the W_2 complex is asymmetrically less distorted than the Mo_2 complex in the solid state.

^1H and ^{13}C NMR spectra of $[W_2(O)_2(\mu\text{-}O)_2(\mu\text{-}rac\text{-pdta})]^{2-}$ in D_2O (Figures S1 and S2) are generally similar to those of $[Mo_2(O)_2(\mu\text{-}O)_2(\mu\text{-pdta})]^{2-}$[7,15] and are consistent with the fixed conformation of the N–C–C(CH_3)–N bridge, as found in the X-ray crystal analysis.

2. Electronic Absorption and CD Spectra. The electronic absorption and CD spectra in water of the present complex together with those of $[Mo_2(O)_2(\mu\text{-}O)_2(\mu\text{-}R\text{-pdta})]^{2-}$[5] are shown in Figure 4. The electronic absorption and CD spectral data for the two pdta complexes in water and in DMF are summarized in Table V. The absorption spectral data of $[W_2(O)_2(\mu\text{-}O)_2(\mu\text{-edta})]^{2-}$ in water are also included. Solvent effects on the absorption and CD spectra are not significant, and the discussions are made on the basis of the spectra in water. The electronic absorption spectrum of $[W_2(O)_2(\mu\text{-}O)_2(\mu\text{-}R\text{-pdta})]^{2-}$ is almost the same as that of $[W_2(O)_2(\mu\text{-}O)_2(\mu\text{-edta})]^{2-}$ both in the position and the intensity of absorption maxima. The spectral patterns of the $Mo_2(O)_2(\mu\text{-}O)_2$ and $W_2(O)_2(\mu\text{-}O)_2$ complexes are very similar if the higher energy shift of that of the latter is considered. Such similarity enables us to classify electronic transitions into groups I–III.[5] From the consideration of the absorption intensities and CD signs, transitions I and II of the W_2 complexes were concluded to be similar in nature to the respective transitions of the molybdenum complexes. Bands I and II of the W_2–*R*-pdta and Mo_2–*R*-pdta complexes are thus characterized by weak and rather strong negative CD bands, respectively. From the absorption intensity, band III of the W_2 complexes is similar in nature to that of the Mo_2 complex. The strong positive CD band observed for the Mo_2–*R*-pdta complex is not seen in the W_2–*R*-pdta complex. It seems that the positive CD band of the W_2–*R*-pdta complex is cancelled out by a negative CD band at slightly higher energy region.

It is seen that CD intensity of the W_2–*R*-pdta complex is generally weaker than that of the Mo_2–*R*-pdta complex. This is particularly clear for band II, in which the corresponding CD band is not superimposed by neighbor CD bands (the smaller intensity is not the result of cancellation by the contribution of a neighbor positive band). Since the CD intensity is expected to reflect the extent of asymmetric distortion, the W_2–*R*-pdta complex has smaller extent of asymmetric distortion as compared with that of the Mo_2–*R*-pdta complex.

3. ^{13}C NMR Dynamic Analysis. The variable-temperature ^1H and ^{13}C NMR spectra of $[Mo_2(O)_2(\mu\text{-}O)_2(\mu\text{-edta})]^{2-}$ indicate rapid conformational inversion of the N–C–C–N bridge, which is equivalent to the interchange of the chemical environment of the acetate arms (Figure 1).[7,15]

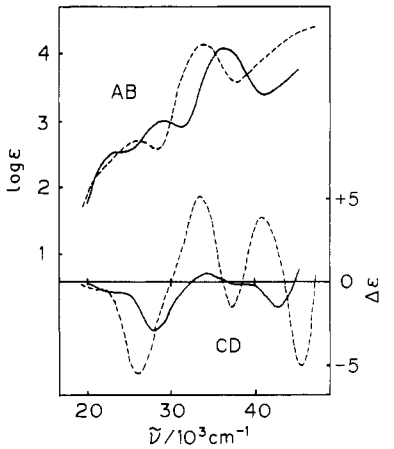

Figure 4. Circular dichroism and electronic absorption spectra of $Na_2[W_2(O)_2(\mu\text{-}O)_2(\mu\text{-}R\text{-pdta})]$ (—) and $Na_2[Mo_2(O)_2(\mu\text{-}O)_2(\mu\text{-}R\text{-pdta})]$ (---) in aqueous solution.

Table V. Electronic Absorption and CD Spectral Data for $[M_2(O)_2(\mu\text{-}O)_2(\mu\text{-}R\text{-pdta})]^{2-}$ (M = W, Mo[a]) and Electronic Absorption Spectral Data for $[W_2(O)_2(\mu\text{-}O)_2(\mu\text{-edta})]^{2-}$[b,c]

complex	I	II	III	medium
(a) Electronic Absorption Data: $\nu/10^3$ cm^{-1} (log (ϵ/M^{-1} cm^{-1}))				
$[W_2O_4(pdta)]^{2-}$	23.8 s (2.54)	29.2 (3.00)	36.1 (4.08)	H_2O
	23.8 s (2.59)	29.2 (3.04)	35.5 (4.00)	DMF[d]
$[Mo_2O_4(pdta)]^{2-}$	20.8 s (2.00)	25.8 (2.60)	33.6 (4.00)	H_2O
		25.6 (2.60)	33.0 (3.99)	DMF[d]
$[W_2O_4(edta)]^{2-}$	23.7 s (2.54)	29.2 (3.04)	36.2 (4.15)	H_2O
(b) CD Data: $\nu/10^3$ cm^{-1} ($\Delta\epsilon$/M^{-1} cm^{-1}))				
$[W_2O_4(pdta)]^{2-}$	22.5 (−0.61)	28.0 (−2.93)	34.2 (+0.57)	H_2O
	22.7 (−0.52)	27.9 (−3.1)	33.2 (+0.40)	DMF[d]
$[Mo_2O_4(pdta)]^{2-}$	20.8 s (−0.48)	26.0 (−5.5)	33.3 (+5.1)	H_2O
	20.6 (−0.38)	25.6 (−6.4)	32.8 (+5.7)	DMF[d]

[a] Reference 5. [b] Reference 15. [c] s indicates shoulder. [d] DMF = *N*,*N*-dimethylformamide.

(14) (a) Khalil, S.; Sheldrick, B.; Soares, A. B.; Sykes, A. G. *Inorg. Chim. Acta* **1977**, *25*, L83–L84. (b) Khalil, S.; Sheldrick, B. *Acta Crystallogr. Sect. B. Struct. Crystallogr. Cryst. Chem.* **1978**, *B34*, 3751–3753.
(15) Haynes, L. V.; Sawyer, D. T. *Inorg. Chem.* **1967**, *6*, 2146–2150.

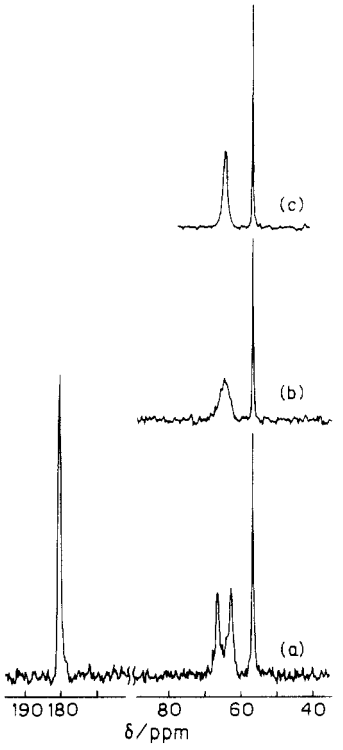

Figure 5. ^{13}C NMR spectra of $Na_2[W_2(O)_2(\mu\text{-}O)_2(\mu\text{-edta})]$ in D_2O at (a) 0 °C, (b) 20 °C, and (c) 35 °C (δ = 0 for DSS).

Figure 5 shows the 22.5-MHz ^{13}C NMR spectra of the $[W_2(O)_2(\mu\text{-}O)_2(\mu\text{-edta})]^{2-}$ complex at 0, 20, and 35 °C. The spectra clearly show the asymmetric inversion in the time scale of ^{13}C NMR spectroscopy. The signals at 0 °C are assigned as follows: sharp signal at 180.5 ppm to carbonyl carbons, broad one at 67.0 and 63.3 ppm to acetate methylene carbons, and sharp one at 56.9 ppm to ethylene carbons. The two broad signals of acetate methylene carbons at 0 °C coalesces to a single peak at the center of two signals at 20 °C. The signal sharpens at higher temperatures. The change indicates an intramolecular conformational (and configurational) inversion (Figure 1).

Spectra at various temperatures (0, 5, 10, 15, 20, 25, 30, and 35 °C) were analyzed by a computer program based on the modified Bloch equation for the two-site exchange.[16] The experimental spectra were digitized. The fitting function and details of analysis are taken from ref 7 and 16. A rate constant at each temperature is provided in the supplementary material. From the temperature dependence of the exchange rates, the enthalpy, $\Delta H^{\ddagger}$, and the entropy, $\Delta S^{\ddagger}$, of activation were evaluated.

(16) Fujiwara, N.; Tomiyasu, H.; Fukutomi, H. *Bull. Chem. Soc. Jpn.* **1984**, *57*, 1576–1581.

Table VI. Rate Constants and Activation Parameters for the Asymmetric Inversion of $[M_2(O)_2(\mu\text{-}O)_2(\mu\text{-edta})]^{2-}$ (M = W, Mo)

	M = W	M = Mo[a]
$k^b/10^2\ s^{-1}$	2.87 ± 0.06	5.1 ± 0.1
$\Delta H^{\ddagger}$/kJ mol^{-1}	36 ± 2	54 ± 8
$\Delta S^{\ddagger}$/J K^{-1} mol^{-1}	−53 ± 5	+12.3 ± 0.2

[a] Reference 7. Since the data treatment in ref 7 involves a mistaken formula ($k_R = 2/\tau$ should read $k_R = 1/2\tau$), the rate constants are corrected appropriately. [b] At 25 °C.

In Table VI the data are compared with $[Mo_2(O)_2(\mu\text{-}O)_2(\mu\text{-edta})]^{2-}$.[7] The $\Delta H^{\ddagger}$ value is appreciably larger for the Mo_2 complex. It seems that the greater amplitude of the conformational inversion of the Mo_2 complex is reflected in the bigger $\Delta H^{\ddagger}$ values. Significant difference in the $\Delta S^{\ddagger}$ values is not easily accounted for, but it would probably reflect the solvational change during the inversion.

Concluding Remarks

The X-ray crystal structures and circular dichroism spectra of the *R*-pdta complexes and asymmetric inversion of the edta complexes are all indicative of the smaller asymmetric distortion of the W_2 complexes than the Mo_2 ones. The difference is small but appreciable. In general, coordination bonds are expected to be of more covalent character for the third-row transition meals as compared with the corresponding second-row transition metals. Perhaps, the somewhat higher extent of covalent character of the metal–ligand bonds of the W_2 complex makes the geometrical structure of the W_2 complex less flexible.

Acknowledgment. We are grateful to Dr. Akira Nagasawa for the measurements and discussions of the NMR spectra and to Dr. Chizuko Kabuto for the crystal structure determination. We are particularly indebted to Masashi Segawa for the initiation of this work and also valuable discussions.

Supplementary Material Available: Figures S1 and S2, showing ^1H and ^{13}C NMR spectra of $[W_2(O)_2(\mu\text{-}O)_2(\mu\text{-}R\text{-pdta})]^{2-}$, and Tables SI–SIV, listing hydrogen atomic coordinates, anisotropic thermal parameters, and bond distances and angles of $Ba[W_2(O)_2(\mu\text{-}O)_2(\mu\text{-}R\text{-pdta})]\cdot 6H_2O$ and rate constants for the asymmetric inversion of $[W_2(O)_2(\mu\text{-}O)_2(\mu\text{-edta})]^{2-}$ (7 pages); tables of calculated and observed structure factors (11 pages). Ordering information is given on any current masthead page.